Land Surface Processes Create Patterns in Atmospheric Residence Time of Water

Tuinenburg, O. A.; van der Ent, R. J.

DOI
10.1029/2018JD028871

Publication date
2019

Document Version
Final published version

Published in
Journal of Geophysical Research: Atmospheres

Citation (APA)
Tuinenburg, O. A., & van der Ent, R. J. (2019). Land Surface Processes Create Patterns in Atmospheric Residence Time of Water. *Journal of Geophysical Research: Atmospheres*, *124*(2), 583-600. https://doi.org/10.1029/2018JD028871

JGR Atmospheres

RESEARCH ARTICLE
10.1029/2018JD028871

Land Surface Processes Create Patterns in Atmospheric Residence Time of Water

O. A. Tuinenburg[1] **and R. J. van der Ent**[2,3]

[1]Copernicus Institute, Faculty of Geosciences, Utrecht University, Utrecht, Netherlands, [2]Department of Water Management, Faculty of Civil Engineering and Geosciences, Delft University of Technology, Delft, Netherlands, [3]Department of Physical Geography, Faculty of Geosciences, Utrecht University, Utrecht, Netherlands

Key Points:
- Land surface affects atmospheric residence time of moisture
- Transpiration has a significantly different atmospheric residence time distribution than canopy evaporation
- The probability of rainout during the first few days after evaporation varies strongly with location

Correspondence to:
O. A. Tuinenburg,
O.A.Tuinenburg@uu.nl

Citation:
Tuinenburg, O. A., & van der Ent, R. J. (2019). Land surface processes create patterns in atmospheric residence time of water. *Journal of Geophysical Research: Atmospheres*, *124*, 583–600. https://doi.org/10.1029/2018JD028871

Received 20 APR 2018
Accepted 28 DEC 2018
Accepted article online 7 JAN 2019
Published online 22 JAN 2019

Abstract Recent studies determined the residence time of moisture in the atmosphere to be 8–10 days but with large spatial and temporal differences. An unexplained daily cycle in the probability density function (PDF) of the residence time of land evaporation was observed, which was not present for oceanic evaporation. Moreover, the PDF of atmospheric residence time of oceanic evaporation was found to be a monotonically decreasing, while for land evaporation, this function had increasing probabilities during the first few days and monotonically decreasing probabilities thereafter. This research determines the causes of (I) the daily cycle in this PDF and (II) the shape of the atmospheric residence time PDF. The strong daily cycle in the residence time PDF using ERA-Interim is attributed to the fact that the evaporation and precipitation have the same diurnal cycle in ERA-Interim. Therefore, evaporation entering the atmosphere has the highest probability of returning to the land surface as precipitation at the same moment during the day but possibly a number of days later. Interestingly, this diurnal cycle was almost absent in the simulations forced with GLDAS surface fluxes. Therefore, we conclude that the previously found daily cycle in the atmospheric residence time PDF is due to differences in the diurnal cycles of precipitation in the underlying data sets. Transpiration causes the increasing probabilities during the first days, while bare soil evaporation and canopy interception typically have a monotonically decreasing PDF. Therefore, we conclude that transpiration causes the largest differences in atmospheric residence time between ocean and land evaporation.

1. Introduction

Although the atmospheric water cycle is routinely simulated with state-of-the-art climate models (e.g., Eyring et al., 2016), some of the most fundamental characteristics of the Earth's water cycle remain largely unknown (e.g., Bony et al., 2015; Shaw et al., 2016). One of these characteristics is how much time water molecules spend in the atmosphere from the moment they evaporate from the Earth surface until the moment they return as precipitation.

The global average time a water molecule spends in the atmosphere is 8–10 days (e.g., Bodnar et al., 2013; Bosilovich & Schubert, 2002; Chow et al., 1988; Jones, 1997; Trenberth, 1998; Van der Ent & Tuinenburg, 2017; Ward & Robinson, 2000; Yoshimura et al., 2004). Only recently, the regional differences in atmospheric residence times have been reported (Läderach & Sodemann, 2016; Van der Ent et al., 2014; Van der Ent & Tuinenburg, 2017; Wei et al., 2016). Van der Ent and Tuinenburg (2017) defined evaporation residence times at location x as the time a water particle at location x will spend in the atmosphere from the moment it evaporates until it returns to the Earth surface as precipitation at any location. They found these evaporation residence times generally to decrease toward areas of high precipitation such as the intertropical convergence zone, and they found evaporation residence times to be generally lower in winter compared to summer.

Based on an off-line atmospheric moisture tracking model, forced with ERA-Interim reanalysis (ERA-I), Van der Ent and Tuinenburg (2017) also showed the probability density functions (PDFs) of the time evaporation remain in the atmosphere before returning to the Earth surface as precipitation. The first 10 days of the PDF have been reprinted here (Figure 1, left). It can be seen that oceanic evaporation was found to be a monotonically decreasing PDF with a mean of 8.1 days and a median of 4.9 days. The PDF of land evaporation had a mean of 10.4 days and a median of 5.1 days, suggesting that oceanic evaporation on average returns

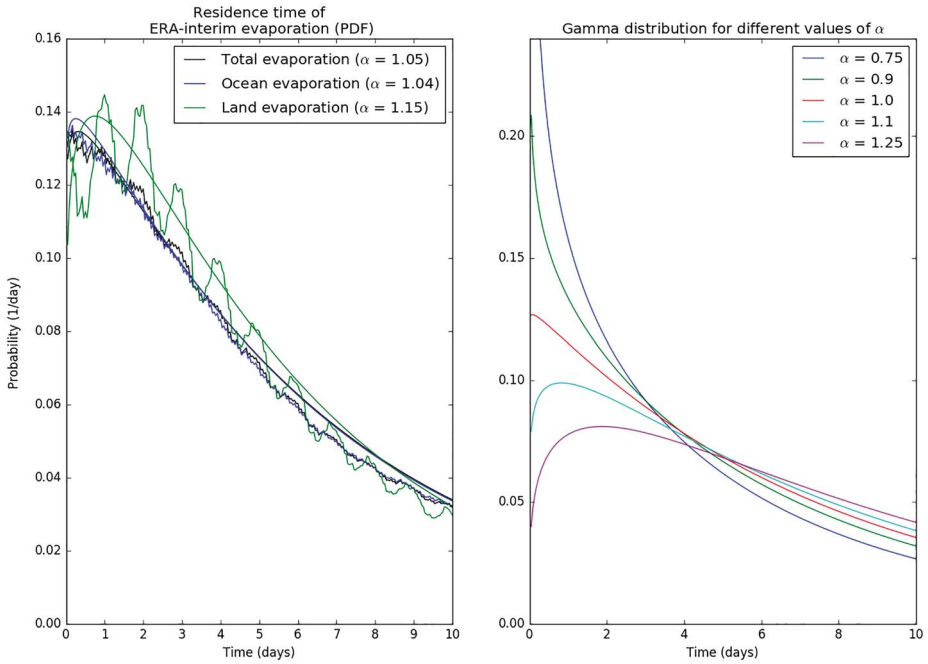

Figure 1. (left) PDF of atmospheric residence time of ERA-I evaporation (Van der Ent & Tuinenburg, 2017), for evaporation from land and ocean surface and all evaporation, with fitted gamma curves and fitted shape components (α) in parentheses. The relative amplitudes of the daily cycle during days 2–4 are 5.8%, 3.7%, and 19.8% for ERA-I total evaporation, ERA-I ocean evaporation, and ERA-I land evaporation, respectively. (right) Gamma distributions for different shape components (α). In this panel, the scale parameter β is fixed at 180 hr (see equation (3)), while in the rest of the paper, it is fitted to the residence time PDFs. PDF = probability density function.

about 2 days quicker to the Earth surface than land evaporation. The PDF of land evaporation also exhibits two distinct phenomena not present in the oceanic evaporation PDF. The first phenomenon is a daily cycle, indicating a higher likelihood for residence times around certain times of the day. The second phenomenon is an increasing PDF in the first few days with a maximum at 1.4 days (calculated with removal of the daily cycle). The (bio)physical mechanisms behind these two phenomena have not yet been explained.

The two main research questions of this paper are (I) Why do we observe a daily cycle in the atmospheric residence time PDF of land evaporation and (II) Which (bio)physical processes cause the differences in the shape of the atmospheric residence time PDFs of oceanic and land evaporation?

We answer these research questions by applying an off-line atmospheric moisture tracking model to total evaporation fluxes from ERA-I (Dee et al., 2011) and separated evaporation components (transpiration, canopy interception, and bare soil evaporation) from GLDAS (Rodell et al., 2004). Then, we fit gamma distributions (Figure 1, right) through the residence time PDFs to characterize the shape of the different PDFs in space and time. We repeat this procedure with MERRA2 (Gelaro et al., 2017) reanalysis to estimate on the robustness of the results. Furthermore, we analyze the daily cycle of evaporation and precipitation in ERA-I and GLDAS to understand the daily cycle in the residence time PDF of land evaporation.

2. Methods

2.1. Moisture Tracking Model

To estimate the atmospheric residence time of surface evaporation and its different components, we used a Lagrangian atmospheric water trajectory model (Tuinenburg et al., 2012, based on Dirmeyer & Brubaker, 2007) that tracks parcels of moisture which are released on random locations within each grid cell, four times every simulated hour. We run the model for each evaporation type (total evaporation, bare soil evaporation, canopy evaporation, and transpiration) separately and assume similar atmospheric behavior for these land surface fluxes. This model is the 3D-T model in Van der Ent and Tuinenburg (2017). The method assumes that evaporation enters the atmosphere 50 hPa (or about 500 m) above the surface pressure. The forward trajectories of these molecules are then forced by linear interpolations of the three-dimensional

ERA-I large-scale wind fields (in u, v, and w directions) and updated every 0.25-hr time step (Δt). This model does not take into account the convective and turbulent wind fields that may redistribute the moisture vertically in the atmosphere, which are not captured by w. Although this vertical moisture redistribution may significantly affect the moisture transport during specific days (Freitas et al., 2000), earlier tests showed that the climatological moisture recycling is well simulated using the current setting and is affected most by the release height (Staal et al., 2018).

During every time step in this trajectory, we allocate some of the moisture in the tracked parcel of water to the current precipitation, scaled with the total precipitable water. Therefore, the amount of allocated precipitation A at a given location x, y and time step t that has previously evaporated at the source location and time can be described by

$$A_{x,y,t} = W_{\text{parcel},t} S_{\text{source}} \frac{P_{x,y,t}\Delta t}{\text{TPW}_{x,y,t}}, \tag{1}$$

where P is the precipitation, W_{parcel} the fraction [−] of the evaporated water still present in the tracked parcel, S_{source} the amount of water in the parcel that evaporated from the source, and TPW is total precipitable water in the atmospheric water column. Every time step, the fraction of original evaporated water in the parcel still present is updated based on precipitation P out of the parcel:

$$W_{\text{parcel},t} = W_{\text{parcel},t-1}\left(1 - \frac{P_{x,y,t}\Delta t}{\text{TPW}_{x,y,t}}\right). \tag{2}$$

Thus, the amount of water that was tracked from the source evaporation area decreases with precipitation along its trajectory. Parcels were followed until either less than 1% of its original amount was left in the atmosphere, or the tracking time was more than 30 days. On average, there was still 5% of the original evaporation present at the moment the simulation was terminated.

2.2. Data

In the preceding study (Van der Ent & Tuinenburg, 2017), the moisture tracking scheme was forced with ERA-I (Dee et al., 2011) land surface fluxes as well as at wind fields and precipitable water. The current study uses the same ERA-I forcing for the wind fields and precipitable water, which are used at the native ERA-I spatial resolution of $0.75 \times 0.75°$, 6 hourly, and 11 vertical levels from 1,000 to 500 hPa with steps of 50 hPa.

In addition to moisture tracking runs with ERA-I data as forcing, in order to determine the atmospheric residence times of different evaporation components, GLDAS 2 (GLDAS Noah Land Surface Model, L4, 3 hourly, $0.25 \times 0.25°$, V2.0; Rodell et al., 2004) and land surface flux products (precipitation, bare soil evaporation, transpiration, and canopy evaporation, as well as the total evaporation) are used over land areas. The GLDAS products are used on their native 3 hourly, $0.25 \times 0.25°$ resolution. Over water surfaces, where GLDAS is not available, the ERA-I surface fluxes are used.

Combining GLDAS surface fluxes with ERA-I atmospheric potentially results in an unrealistic combination of evaporation and precipitation with atmospheric dynamics, because the forcing data of the GLDAS data set is not exactly similar to ERA-I. To test whether this impacts the analysis, we repeated the simulations using forcing data from MERRA2 (Gelaro et al., 2017) on its native spatial resolution of $0.5 \times 0.625°$, with 16 vertical levels between 1,000 and 500 hPa.

Three hourly ($0.25 \times 0.25°$) TRMM precipitation data (version 3B42; Huffman et al., 2007) is used to compare the diurnal cycles of precipitation over regions in the Congo and Amazon basins. All simulations in this study were done for moisture released from January to December 2005 (potentially running through January 2006).

2.3. Gamma Function

For each grid cell, the moisture tracking model provides a PDF of the atmospheric residence time of the evaporation from that grid cell (the curves in Figure 1). Empirically and theoretically, the gamma function (equation (3)) has been shown to fit distributions of average residence times of the outflow from catchments relatively well (Benettin et al., 2017; Berghuijs & Kirchner, 2017; Hrachowitz et al., 2010; McGuire & McDonnell, 2006). In order to characterize these curves, a gamma function (equation (3)) was fitted to this PDF, disregarding the first 6 hr of the PDF to improve the stability of the fitting. Although we fully admit

that the real residence times can differ from being gamma distributed, we consider the gamma function to be useful for characterization.

$$f(x;\alpha,\beta) = \frac{\beta^{\alpha}x^{\alpha-1}e^{-\beta x}}{\Gamma(\alpha)}, \tag{3}$$

for $x, \alpha, \beta > 0$, and with $\Gamma(\alpha)$

$$\Gamma(\alpha) = \int_0^{\infty} x^{\alpha-1}e^{-x}\,\mathrm{d}x. \tag{4}$$

Our analysis focuses on the α values of this fit, which influence the shape of the curve (see Figure 1, right). The β values only influence the scaling of the distribution. The average standard error in the fit of α was 0.0511 for ERA-I and 0.050 for the total GLDAS evaporation. The standard error for the GLDAS canopy evaporation, bare soil evaporation, and transpiration was 0.055, 0.049, and 0.044, respectively. The mean residence times are all around 8 days in this study; therefore, the β values are all similar (around 180 hr), and we will not focus on these in this study.

2.4. Daily Cycle

The daily cycle present in the PDF is determined based on the first few days of the PDF. For each hour of these days, the local (linear) trend of the PDF was subtracted from the PDF values. For each hour in the PDF, the daily cycle is the ratio of the standard deviation and the mean of the detrended PDF for the following 24 hr. The mean was taken over days 2–4 (hours 24 to 96) to determine a representative value for the daily cycle. We excluded the first day of the PDF, because the trends during the first day are typically large.

2.5. Lag Between Evaporation and Precipitation

The cause for a large daily cycle in the atmospheric residence time PDF could be that there is a preferential time of day for evaporation and precipitation. If water enters the atmosphere at this preferential evaporation time and leaves the atmosphere at this preferential precipitation time, there will be a strong daily cycle in the residence time. Therefore, the daily cycles of surface fluxes are determined for ERA-I and GLDAS. For individual grid cells, the time lag between the daily cycles of the evaporation and precipitation fluxes was determined. This local lag is a first-order approximation, as in reality evaporated moisture would be advected downwind and potentially rain out over a different grid cell.

The lag between evaporation and precipitation is analyzed on two time scales. First, it is assessed on the daily time scale to assess its influence on the daily cycle of the atmospheric residence time. Second, it is assessed on the time scale of the atmospheric residence time of moisture, up to 30 days (95% of the moisture accounted for). On the daily time scale, the PDF of local lag between evaporation and precipitation is determined by summing all products of E and P for a lag l:

$$\sum_{t=0}^{t=23} E_t * \Delta t * P_{(t+l)} * \Delta t, \tag{5}$$

in which t is the hour of day, $\Delta t = 1$ hr, and 24 hr is subtracted if $t + l > 23$ hr. This is done for all lags from 0 to 23 hr, and the resulting PDF is normalized. The lag PDF is calculated based on hourly surface flux data. GLDAS and ERA-I surface fluxes are linearly interpolated to hourly values.

Subsequently, the standard deviation of this lag PDF is used as a measure for the likelihood of the evaporation and precipitation timing as a cause for the daily cycle in the atmospheric residence time and analyzed globally. The amount of precipitation after evaporation events is determined by taking the global sum of

$$\frac{\sum_{t=0}^{t=365*24} E_t * \Delta t * P_{(t+l)} * \Delta t}{\sum_{t=0}^{t=365*24} E_t * \Delta t}, \tag{6}$$

where t is the hour of year, $\Delta t = 1$ hr, and l is the lag between evaporation and precipitation. This is done for lags up to 30 days.

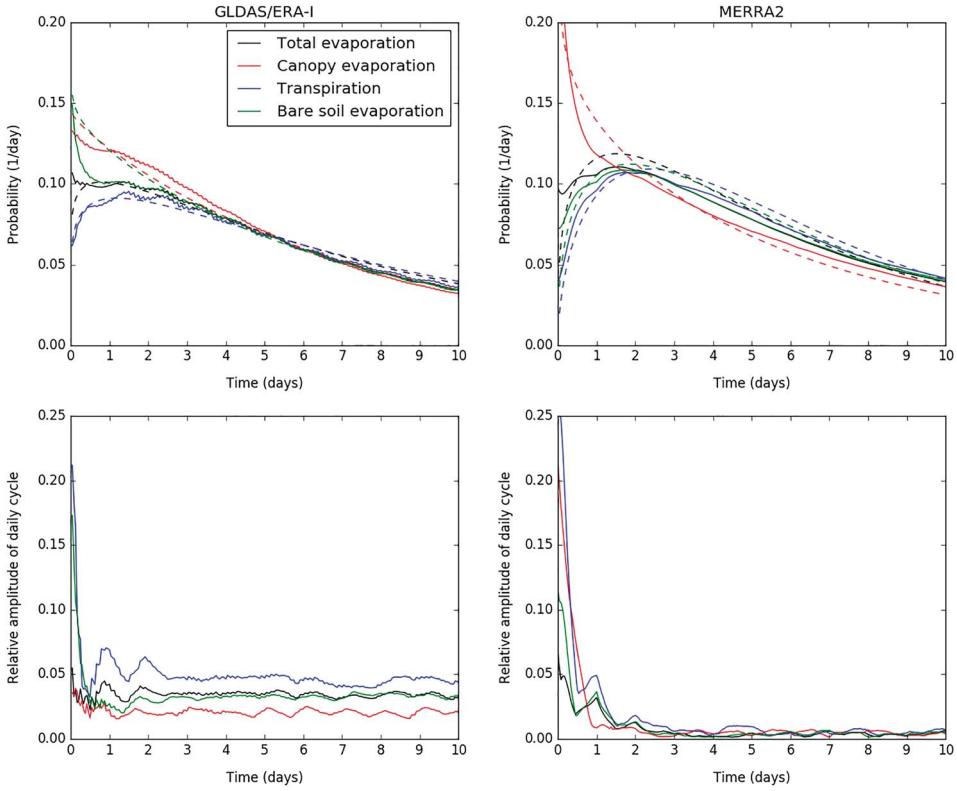

Figure 2. Global and annual mean atmospheric residence times of different GLDAS (top left panel) and MERRA2 (top right panel) evaporation components, with gamma distribution fitted and plotted in dashed lines. GLDAS; total evaporation ($\alpha = 1.11$, $\beta = 176$), canopy evaporation ($\alpha = 0.99$, $\beta = 174$), transpiration ($\alpha = 1.16$, $\beta = 180$), and bare soil evaporation ($\alpha = 0.96$, $\beta = 185$). MERRA2; total evaporation ($\alpha = 1.32$, $\beta = 171$), canopy evaporation ($\alpha = 0.90$, $\beta = 174$), transpiration ($\alpha = 1.56$, $\beta = 182$), and bare soil evaporation ($\alpha = 1.4$, $\beta = 173$). (bottom panels) Magnitude of daily cycle in the probability density functions in the top panel. The relative amplitude of this daily cycle during days 2–4 of the PDF are 3.5%, 2.0%, 5.0%, and 2.9% for GLDAS total evaporation, canopy evaporation, transpiration, and bare soil evaporation and 0.8%, 0.5%, 1.3%, and 0.8% for MERRA2 total evaporation, canopy evaporation, transpiration, and bare soil evaporation.

3. Results

This section presents the analysis of the atmospheric residence time of evaporation, based on moisture tracking simulations with three forcing data configurations. In the first configuration, the moisture tracking model is forced with ERA-I data for both the atmospheric variables (wind and humidity fields) and the surface fluxes (precipitation and evaporation). In the second configuration, the model is forced with ERA-I data for the atmosphere but with different components of the GLDAS surface flux data over land. To test the robustness of the results, the model is forced with the MERRA2 reanalysis in the third configuration.

The results from the second and third configurations, the annual mean global average atmospheric residence time PDF of the GLDAS and MERRA2 evaporation components in Figure 2, are quite different from those of the first configuration (Figure 1, left). The amplitude of the daily cycle of the PDFs is much smaller than those of the ERA-I forcing. Furthermore, the shape of the atmospheric residence time PDF is different for the different GLDAS and MERRA2 evaporation components. The GLDAS PDFs of canopy and bare soil evaporation are monotonically decreasing with time, while that of transpiration is increasing during the first 2 days. Based on the MERRA2-forced simulations (Figure 2, right panels), the daily cycles are much smaller than those of the ERA-I and ERA-I/GLDAS-forced simulation. However, the shape of the PDFs for the evaporation components are similar to those of the ERA-I/GLDAS-forced simulations. The differences in atmospheric residence time of evaporation between the two configurations and their causes are analyzed in terms of its daily cycle in section 3.1 and the shape of the PDF in section 3.2.

3.1. Daily Cycle

3.1.1. Daily Cycle for Different Evaporation Components

The amplitude of the daily cycle of the global-averaged atmospheric residence time PDF (bottom panel of Figure 2) of transpiration is about two times larger than those of bare soil and canopy evaporation. For all components, the amplitude of the daily cycle decreases with time after the moment of evaporation, which is also the case for the simulation forced with ERA-I. This means that during the first few days after evaporation, moisture is more likely to rain out at specific times during the day. After a couple of days in the atmosphere, the moisture is transported away from the evaporation location. This transport may occur in different directions, where the daily cycle of the land surface fluxes may be different. Therefore, the moisture has a more equal probability of rainout during all hours of the day, and the daily cycle in the atmospheric residence time PDF decreases with time.

The magnitude of the diurnal cycle is smaller for all evaporation components in GLDAS than it is for ERA-I (in this study we use daily cycle to describe the fluctuations of the atmospheric residence time with a period of 1 day. We use diurnal cycle to indicate the different probability of evaporation and precipitation during different moments of the day). With about 5% of the signal, the magnitude of the diurnal cycle in GLDAS is around four times smaller than it is for ERA-I. This difference in diurnal cycle cannot be explained by a different distribution of evaporation across its components (transpiration, bare soil evaporation, and canopy evaporation) between ERA-I and GLDAS, as all GLDAS components have a lower diurnal cycle amplitude than ERA-I evaporation.

Apart from these differences in globally averaged daily cycle of residence time, there are some spatial differences in this daily cycle. As a measure of this daily cycle, Figure 3 shows the ratio between the standard deviation and the mean of the detrended PDF of atmospheric residence time between days 2 and 4. Note that the analysis in Figure 3 is done for the PDF per grid cell, whereas that in Figure 2 is done for the global PDF. There is more variability in the PDF per grid cell than for in the global mean. This is due to numerical averaging that reduces the variability but also due to local features such as nearby mountain ranges causing precipitation peaks. Therefore, the values for the daily cycle per grid cell will be larger than the global mean value.

Over all extratropical land masses, the magnitude of the daily cycle has similar values for ERA-I and GLDAS, with the exception of central Asia, where the daily cycle in GLDAS is larger than in ERA-I. Figure A1 in Appendix A shows a difference plot of the two panels in Figure 3.

However, the daily cycles in the tropics differ between these two forcing data sets. The magnitude of the daily cycles in GLDAS are typically a factor 2 to 3 lower than the magnitudes in ERA-I in the tropics, with typical tropical values of 0.05–0.1 for GLDAS and 0.2–0.25 for ERA-I.

The daily cycles in the MERRA2 simulations are not similar to either ERA-I or ERA-I-GLDAS. In South America, MERRA2 has the higher daily cycles present in ERA-I, while in tropical Africa, MERRA2 has the lower values of GLDAS. In contrast with the global mean, the MERRA2 simulation have a relatively strong daily cycle on the individual grid cell level. The global mean value of the strength of the MERRA2 daily cycle is between those for ERA-I and ERA-I-GLDAS.

3.1.2. Diurnal Cycle of Land Surface Fluxes in ERA-Interim and GLDAS

To determine the cause of this large tropical difference in daily cycle of the atmospheric residence time of evaporation, the land surface fluxes and atmospheric moisture residence time of two subregions (in parts of the Congo and Amazon, see boxes in Figure 3) are analyzed in more detail. Only land grid cells within these subregions were used in the analysis. Figure 4 shows the atmospheric residence time PDFs of ERA-I and GLDAS evaporation from both these regions. There is a clear difference in amplitude of the daily cycle; it is much larger in ERA-I than in GLDAS.

The cause of this large difference in daily cycle appears to be the difference in timing of the evaporation and precipitation during the day for ERA-I and GLDAS. Figure 5 shows the annual mean diurnal cycles in precipitation and evaporation (and its different components for GLDAS) for the Congo and Amazon regions. The strong diurnal cycles of evaporation in ERA-I correspond quite well to those in GLDAS. Moreover, the diurnal cycles of the GLDAS evaporation components (transpiration, canopy evaporation, and bare soil evaporation) are similar to the total GLDAS and ERA-I diurnal cycles.

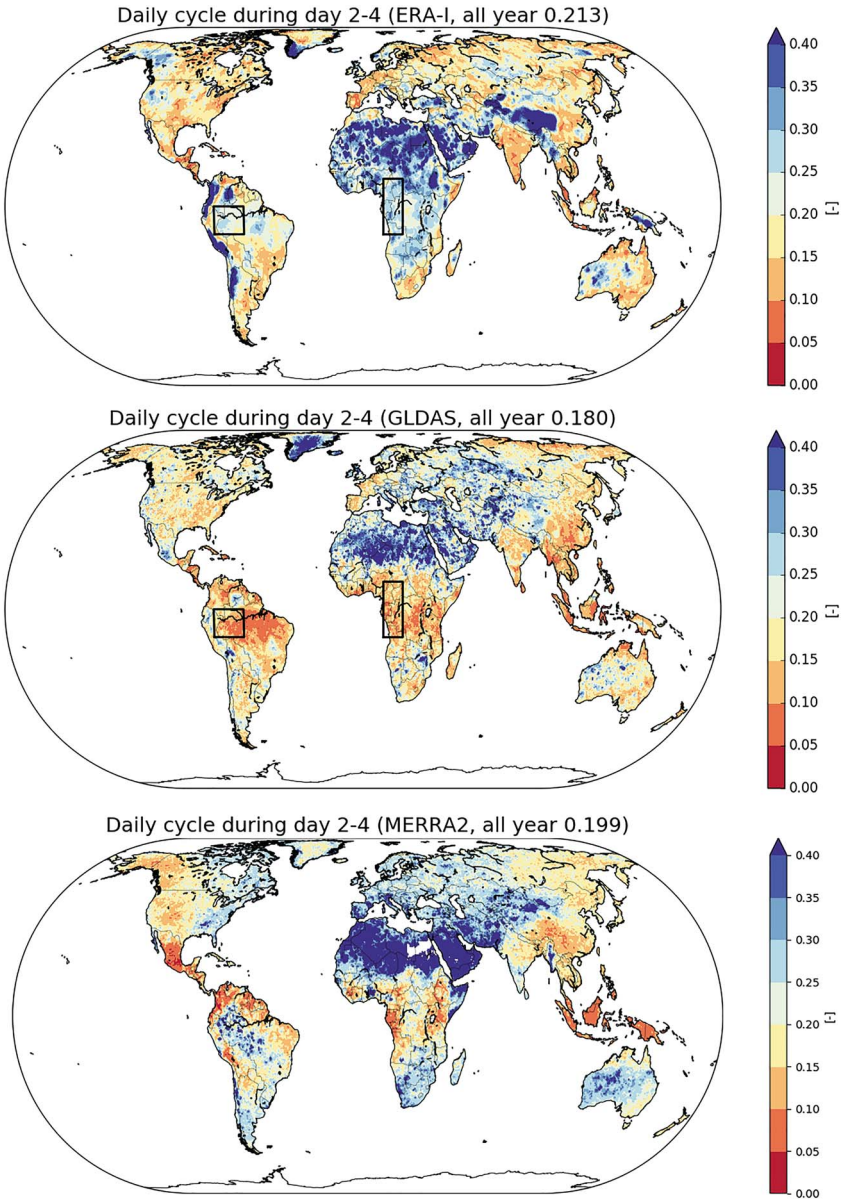

Figure 3. Relative amplitude of daily cycles of probability density functions of atmospheric residence time for days 2–4 of the trajectory (volume-weighted annual mean), for ERA-I (top), GLDAS (middle), and MERRA2 (bottom). The regions indicated in the rectangle correspond to regions in Figures 4 and 5. ERA-I = ERA-Interim.

However, the ERA-I and GLDAS diurnal cycles of precipitation are very different. In ERA-I, there is a strong peak in precipitation around noon, whereas the GLDAS precipitation is distributed (almost) uniformly throughout the day. For these two regions, the GLDAS precipitation diurnal cycle resembles the TRMM precipitation (which is plotted as a reference) better than the ERA-I precipitation does. The daily cycles of precipitation and evaporation are determined for four additional regions in Appendix A. Furthermore, Appendix A shows that the precipitation daily cycles of TRMM and ERA-I are more similar in other regions of the world, while the amplitude of the GLDAS precipitation daily cycle is lower than that of TRMM almost everywhere.

If evaporation that enters the atmosphere is assumed to be subject to the diurnal cycles in precipitation in Figure 5, we can determine a PDF of the lag between evaporation and precipitation, based on these diurnal cycles. This assumption is probably realistic during the first few days in the atmosphere but not anymore if

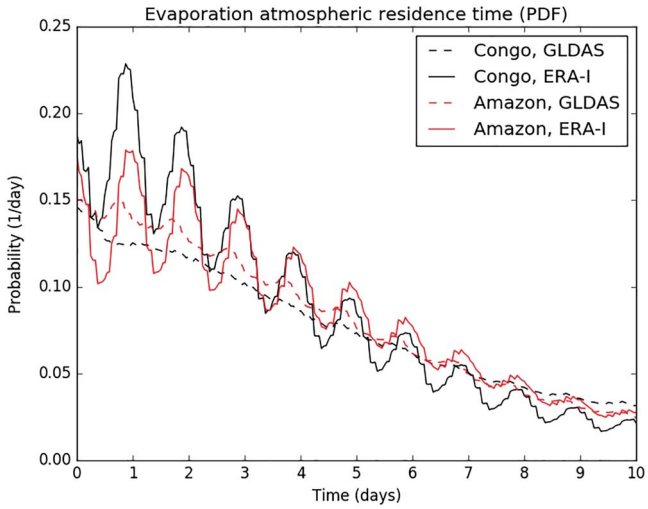

Figure 4. PDF of atmospheric residence time of ERA-I and GLDAS (total) evaporation, for the Congo and Amazon regions (see Figure 3 for regions). ERA-I = ERA-Interim; PDF = probability density function.

the moisture is transported away from the source area where different diurnal cycle of land surface fluxes are present.

This lag PDF is plotted in black curves in Figure 5 (on the right vertical axis). The diurnal cycle in this lag PDF is large if there is a preferential time difference between the evaporation and precipitation daily cycles. This preferential time difference occurs only if there are daily cycles in both evaporation and precipitation. In that case, evaporation enters the atmosphere preferentially at one moment ($time_e$), and this moisture leaves the atmosphere preferentially during a subsequent moment ($time_p$), giving a preferential atmospheric residence time of $time_p - time_e$.

For ERA-I fluxes, there is a diurnal cycle in the lag PDF: the probability that there is a 12-hr (plus a multiple of 24 hr) lag between evaporation and precipitation is two to three times lower than the probability of a 0-hr (plus a multiple of 24 hr) lag. This means ERA-I evaporation has larger probability of raining out at moments of the day which are a multiple of 24-hr moment of evaporation. Therefore, we expect a strong daily cycle in the atmospheric residence time of ERA-I evaporation. For GLDAS, the lag PDF is fairly constant: there is almost no preferential lag between evaporation and precipitation. This is true for all GLDAS components, the lag PDFs of the components overlap and are barely distinguishable in Figure 5. Therefore, the daily cycle of the atmospheric residence time of GLDAS evaporation is much weaker for the Congo and Amazon regions.

This difference in lag PDF between ERA-I and GLDAS is present throughout the tropics. Figure 6 shows the standard deviation of this lag PDF per grid cell. In the tropics, this standard deviation, and thus the $E - P$ lag induced daily cycle in atmospheric evaporation residence time, is much larger for ERA-I than for GLDAS, with the MERRA2 standard deviation corresponding more to ERA-I. In extratropical areas, the two data sets are much more similar. North of 50° N, the standard deviations of the lag PDF of GLDAS fluxes increase abruptly, most likely due to the different precipitation data that is assimilated there.

3.2. Shape of Evaporation Residence Time PDF

As shown in Figure 1, the shape of the atmospheric residence time PDF is different for evaporation from land than for evaporation from oceans. For evaporation from oceans, the PDF is monotonically decreasing from the moment of evaporation. In contrast, for evaporation from land, the PDF has increasing probabilities of rainout during the first 2 days after release into the atmosphere. Only after these initial few days, the probabilities decrease again. We analyze the shape of the PDF by fitting a gamma distribution to it (see equation (3)). The shape of a gamma distribution is determined by the α parameter. Figure 1 shows the different shapes of the distribution for different values of this α parameter. For $\alpha \leq 1$, the distributions are monotonically decreasing, while for $\alpha > 1$, probabilities first increase before decreasing.

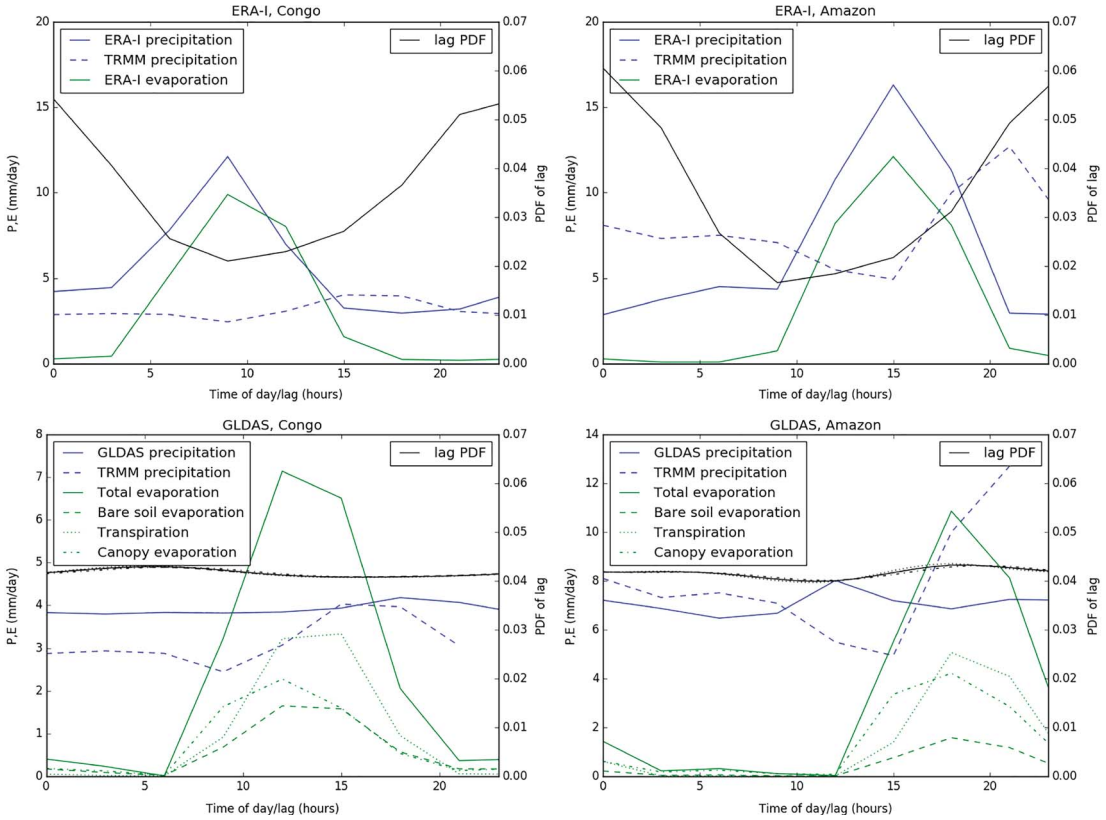

Figure 5. Precipitation (blue lines) and evaporation (green lines) products for the Congo (left column) and Amazon (right column) regions (see Figure 3 for regions), for ERA-I (upscaled to one value per hour, top row) and GLDAS (bottom row) products. Based on precipitation and evaporation, a PDF of the lag between evaporation and precipitation is plotted in black (and on the right axes). The standard deviation of these lag PDFs are 0.01848 (Congo, GLDAS), 0.30816 (Congo, ERA-I), 0.02400 (Amazon, GLDAS), and 0.04013 (Amazon, ERA-I). For GLDAS, this is the standard deviation of the lag PDF based on the total evaporation. ERA-I = ERA-Interim; PDF = probability density function.

3.2.1. Shape Factor α for Different GLDAS Evaporation Components

The parameters of the gamma distribution fit to the global residence time PDFs of GLDAS evaporation components are shown in the legend of Figure 2. The PDFs of the different evaporation components have different shapes. Canopy evaporation and bare soil evaporation have monotonically decreasing PDFs ($\alpha < 1$), while the PDF of transpiration increases until day 2, after which it decreases ($\alpha = 1.18$). The total GLDAS evaporation has a PDF with a gamma distribution fit with $\alpha = 1.09$, roughly corresponding to the shape of the ERA-I PDF.

Figure 7 shows the fit of the gamma distribution to the mean residence time PDF per grid cell. The α values of these fits are similar for ERA-I and GLDAS, except in some parts of southern South America. MERRA2 has lower values for α in India, the maritime continent, and Mexico as well as the northern parts of America and Eurasia.

Across the data sets, high values of α are found in dry areas. In these areas, there is limited precipitation. Therefore, any evaporation is likely to be transported out of the area until it will be part of a downwind precipitation event a few days later. As a consequence, the probability of rainout will initially increase with time, resulting in values of $\alpha > 1$. However, because the total evaporation is limited in dry areas, these will not contribute much to the global mean residence time PDFs in Figures 1 and 2.

There are some areas with large evaporation rates that have relative high α values, notably the Amazon and India. Higher α values are likely due to the nearby mountain ranges (the Andes for the Amazon and the Himalayas for India), although it should be noted that the values for India are much lower in MERRA2. In the seasons that the wind direction is toward the nearby mountain ranges, any evaporation from the Amazon and India will be transported by the wind toward the mountains, where it has a high probability of raining out. Because this transport typically takes some days (Tuinenburg et al., 2012; Van der Ent & Savenije, 2011;

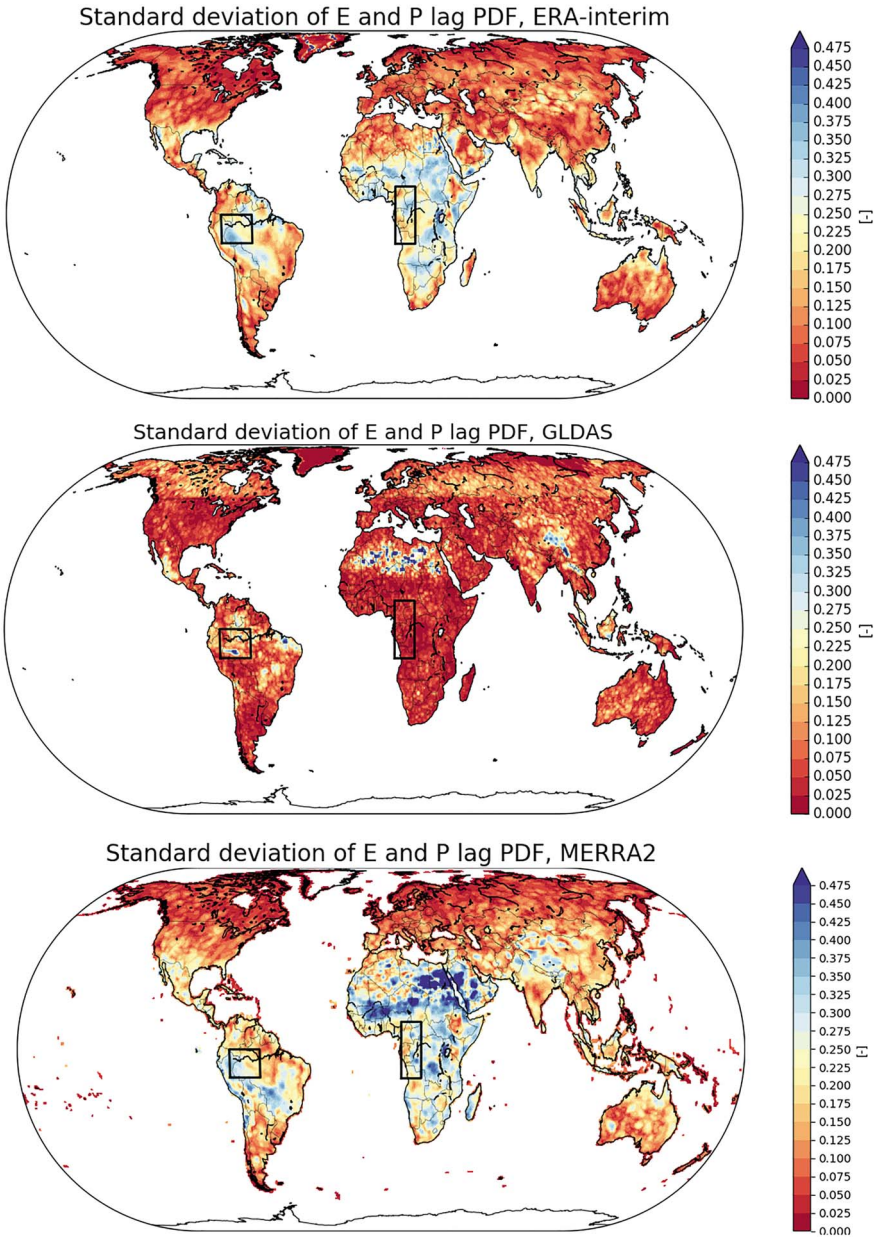

Figure 6. Standard deviation of the PDF of lag between evaporation and precipitation for ERA-Interim (top, global mean: 0.139), GLDAS (bottom, global mean: 0.072), and MERRA2 (global mean: 0.176). The standard deviations of ERA-Interim and GLDAS correspond to the standard deviation of the black lines in Figure 5. PDF = probability density function.

Van der Ent et al., 2014), there is a higher probability of rainout some days after evaporation and hence larger values of α for the gamma distribution fit.

The fitted values of α for the GLDAS and MERRA2 evaporation components in Figure 8 have a similar spatial pattern as the total evaporation for both data sets (Figure 7). Despite these similar spatial patterns, the α values for transpiration are generally higher than for bare soil and canopy evaporation for both GLDAS and MERRA2.

The zonal mean values of α in Figure 9 are typically higher for transpiration than for the other components. In the extratropics, the α values of the fits vary seasonally. In summer, α is generally higher than in winter for all evaporation components but especially for bare soil and canopy evaporation. For the winter and spring seasons, α values for transpiration are only slightly lower than in summer.

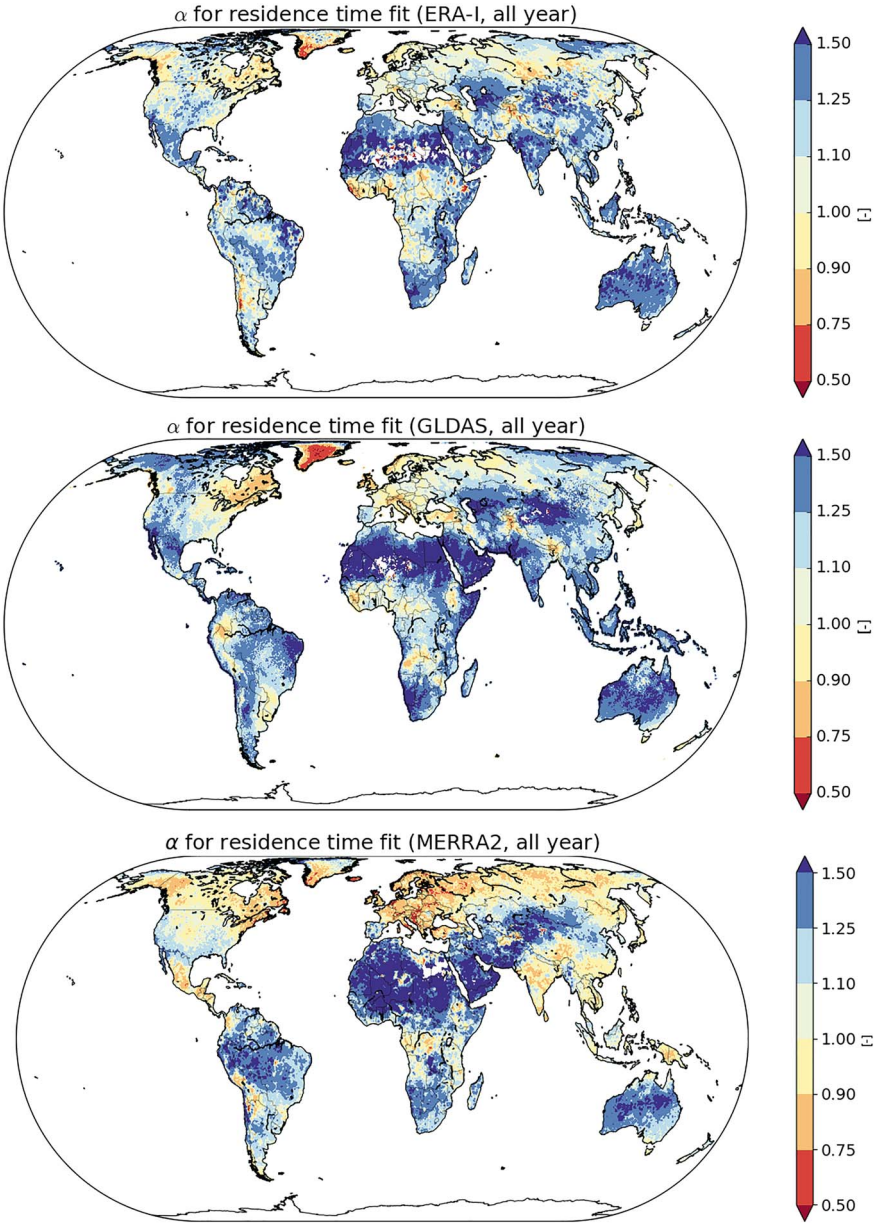

Figure 7. Annual mean fitted values for gamma distribution shape component (α) for ERA-I (top), GLDAS (middle), and MERRA2 (bottom). ERA-I = ERA-Interim.

3.2.2. Evaporation-Precipitation Lag for Different GLDAS Evaporation Components

Given the different shape factors α for the different GLDAS evaporation components (Figures 2 and 8), it is interesting to assess the amount of precipitation after evaporation events. This is shown in Figure 10 for each GLDAS evaporation component. Note that Figure 10 shows the probability of precipitation at the same location as the preceding evaporation. Therefore, the same caveat applies as for the lag PDFs in Figure 5, this amount is valid during the first few days after evaporation but may become less certain at longer lags, as the atmospheric moisture is transported away from the evaporation location.

During the first 2 days after evaporation, there is a strong difference in precipitation amount between the different evaporation components. Immediately after evaporation from the canopy, there is more precipitation than after bare soil evaporation and transpiration. Canopy evaporation has a higher probability of raining out in the 2 days after evaporation than in the days after day 2. For transpiration, the opposite is true and has a lower probability of raining out during the first 2 days than during the days after day 2, while there is

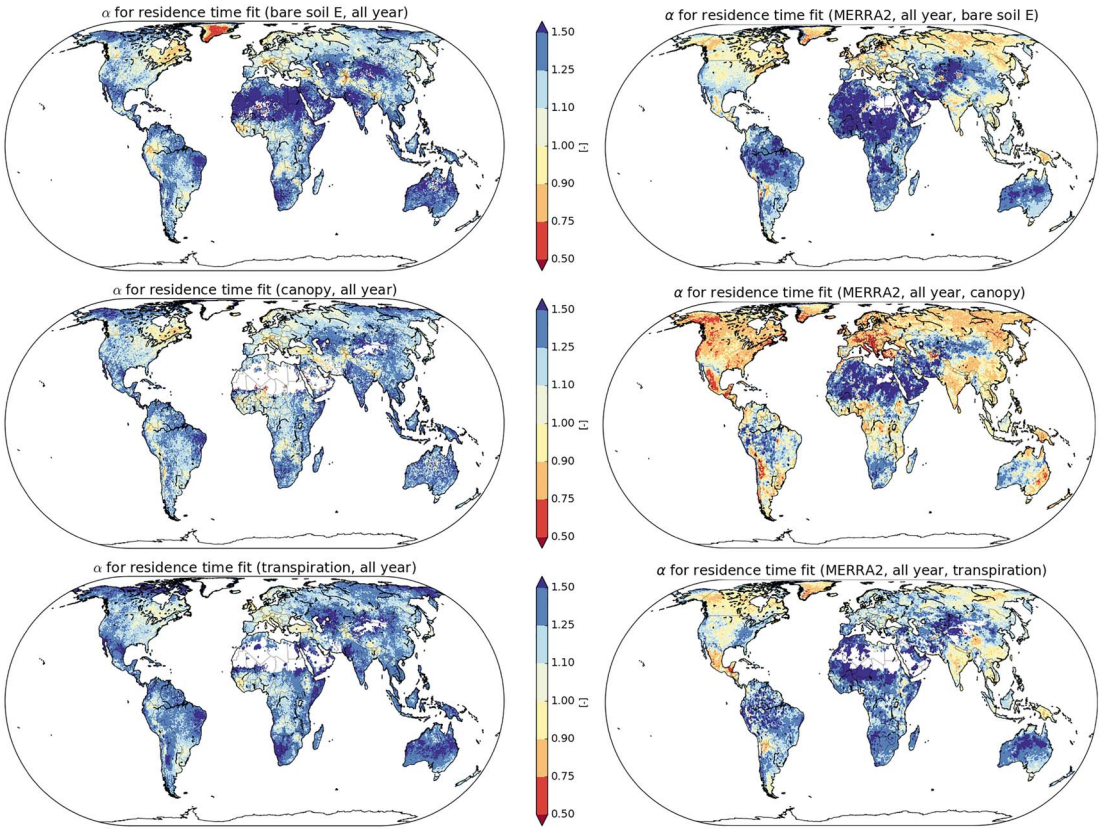

Figure 8. Fitted values for gamma distribution shape component (α) per GLDAS (left column) and MERRA2 (right column) evaporation type: bare soil evaporation (top), canopy evaporation (middle), and transpiration (bottom).

no real preferential precipitation moment for bare soil evaporation and the total GLDAS evaporation. The steady state that is reached after about 3 days is different for each type of evaporation due to the fact that these types occur preferentially in different places. Canopy evaporation tends to occur in location with more precipitation than the other types of evaporation.

This precipitation PDF reflects the different water reservoirs from which these evaporation processes draw their water. The canopy reservoir is small and filled during precipitation events, increasing the probability

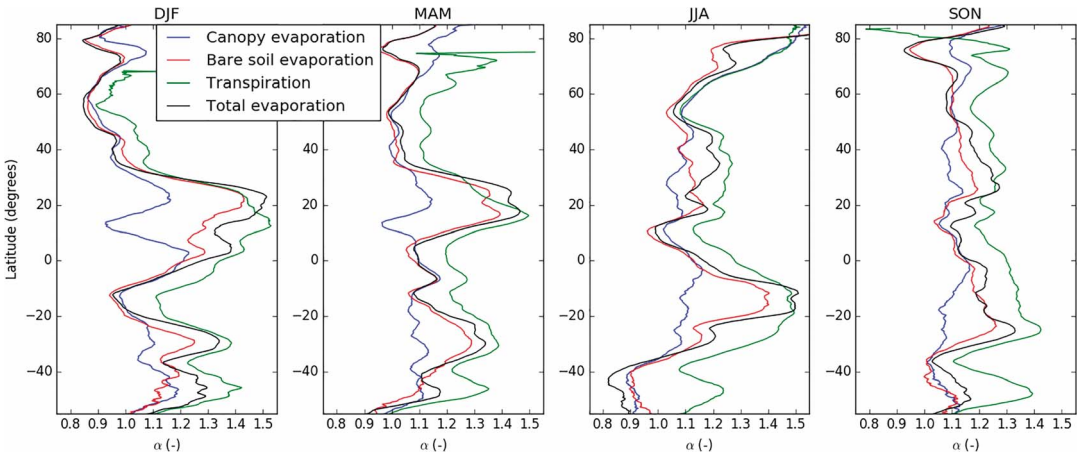

Figure 9. Mean zonal values for α: the shape factor of the gamma distribution (see Figure 1, right), per season and GLDAS evaporation component. DJF = December-January-February; MAM = March-April-May; JJA = June-July-August; SON = September-October-November.

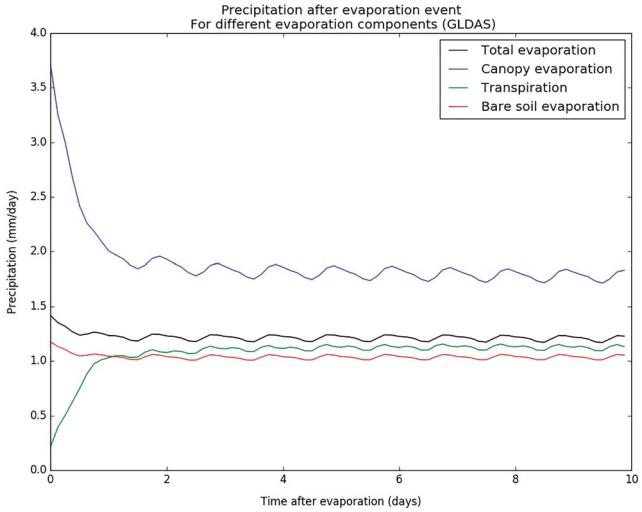

Figure 10. Precipitation after different evaporation types, based on GLDAS precipitation and evaporation component. Global annual mean, in which the precipitation is weighed with the amount of evaporation during each evaporation event. Note that this is the precipitation at the location of evaporation, which may not be comparable to Figure 2 after several days, because the evaporation has been transported downwind.

that canopy evaporation occurs during atmospheric conditions favorable for precipitation. Transpiration draws from the total plant root zone, a much larger reservoir, that is filled up during longer periods (e.g., Wang-Erlandsson et al., 2016). Given the larger reservoir size, the bulk of the transpiration will occur during atmospheric conditions favorable for evaporation, which tend to be days without precipitation. Therefore, the fact that canopy evaporation is driven by the moisture supply and the transpiration is driven by atmospheric demand influences the atmospheric residence time of moisture.

4. Discussion

The analyses and characterization of the atmospheric moisture residence time in this study have underlying assumptions and uncertainties that potentially influence the results significantly. The following subsections assess these influences for the daily cycle and partitioning in surface flux data and the moisture tracking model. We assess the uncertainty in the surface flux data to have the largest influence on our results.

4.1. Daily Cycle and Partitioning of Land Surface Fluxes

The representation of the diurnal cycle of land surface fluxes (evaporation and precipitation) in the forcing data is a large source of uncertainty for the estimation of the daily cycle of atmospheric residence time in the current study. There is a large variability in the diurnal cycle between models and data products, as illustrated for the Amazon and Congo in Figure 5. Typically, atmospheric models have a diurnal cycle of precipitation that mismatches with observations. In the models, precipitation typically occurs around midday, while in observations, the peak occurs later in the day at the end of the afternoon or in the evening (Betts & Jakob, 2002; Dai et al., 1999; Dirmeyer et al., 2012; Trenberth et al., 2003). The diurnal cycle of evaporation is also quite different for ERA-I and GLDAS (Figure 5). In ERA-I, the evaporation peak coincides with the precipitation peak around midday, while the GLDAS evaporation occurs about 2 hr later, during the midafternoon. There are some studies that have looked at comparing the diurnal cycle of observed and modeled evaporation (e.g., Blyth et al., 2010). However, there are few global studies of the diurnal cycle of evaporation to compare these modeled diurnal evaporation cycles, and this is in fact an outstanding research question (Fisher et al., 2017). The diurnal cycle of both precipitation and evaporation in the forcing data has a large influence on the estimates of the daily cycle of atmospheric residence times. Therefore, we conclude that the strong daily cycle found in Van der Ent and Tuinenburg (2017) is likely an artifact of the ERA-I surface flux forcing data.

Apart from the diurnal cycle in the forcing data, the components of evaporation (bare soil evaporation, canopy evaporation, and transpiration) from GLDAS are used to determine the residence time of each of these components separately. Although the separation of the total evaporation into its components varies

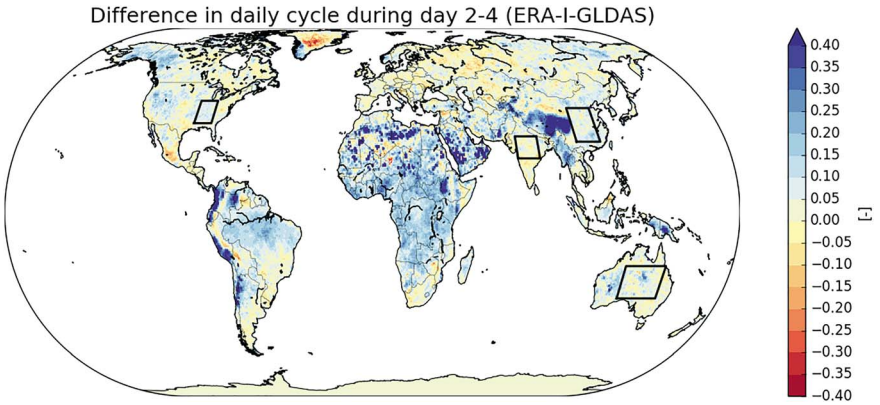

Figure A1. Difference in amplitude of the daily cycle of the probability density functions of atmospheric residence time for days 2–4 of the trajectory (annual mean), for ERA-I minus GLDAS (see Figure 3 for absolute values). The regions indicated in the rectangle correspond to regions in Figure A2. ERA-I = ERA-Interim.

between hydrological models (Dirmeyer et al., 2006) and is quite uncertain (Coenders-Gerrits et al., 2014; Schlesinger & Jasechko, 2014; Sutanto et al., 2014), the GLDAS fraction of transpiration to total evaporation (0.44 with a standard deviation of 0.05, based on monthly mean values) is in line with estimates in Schlesinger and Jasechko (2014)

A further uncertainty of the combination of GLDAS surface fluxes with ERA-I atmospheric data is that GLDAS surface fluxes have been determined using different atmospheric data than ERA-I. Despite the fact that both data sets simulate the same historical days, there may have been differences between the atmospheric variables in the GLDAS forcing data and ERA-I. For example, if there is an underestimation of the atmospheric humidity in the GLDAS forcing data, an overestimation of GLDAS evaporation is expected. Although the current paper takes annual means, there could be a bias in the estimated residence time if there is a systematic difference between the GLDAS atmospheric forcing and ERA-I.

By repeating the simulations with the MERRA2 forcing data set, we found similar results for the shape of the residence time PDF for different evaporation components compared to the ERA-I/GLDAS simulations. Transpiration is related to higher values of α than bare soil evaporation and especially canopy evaporation. The daily cycle in the global PDF was almost absent in the MERRA- forced simulations, while this cycle is present in the PDFs of the MERRA2 individual grid cells. This indicates that the daily cycles in MERRA2 are not synchronous when the grid cells are aggregated into regional clusters or even globally. This difference between MERRA2 and ERA-I/GLDAS could be due to the higher spatial and temporal resolutions of the data set. This could be explored in future work; for the current work, it confirms that this daily cycle varies strongly with the forcing data.

4.2. Moisture Tracking Model

Any off-line atmospheric moisture tracking model deals with uncertainties with respect to the forcing data and the assumptions taken in the model. As discussed, the uncertainties in the forcing of the surface fluxes translate into significant uncertainties in the residence time PDFs. Next to these surface fluxes, the moisture tracking model is forced with three-dimensional data of wind and humidity. We estimate that the choice of the three-dimensional atmospheric forcing data set has a smaller impact on the results of our study than that of the surface fluxes. Climatological moisture footprints, so-called evaporation sheds (Van der Ent & Savenije, 2013), are similar for the moisture tracking model forced with MERRA reanalysis (Rienecker et al., 2011) and ERA-I (Keys et al., 2014). So we assume these footprints to be not very sensitive to the atmospheric forcing data set used, although we did not repeat the procedure with an alternative forcing data set.

During the moisture tracking, assumptions about the initial vertical position of the moisture parcels and their vertical displacement during the simulation could have an impact on the atmospheric residence times. These assumptions seem to be especially important during periods of high vertical shear (Van der Ent et al., 2013) but are probably less important for the long-term mean results of the current study. This is confirmed by some sensitivity tests to including vertical convective motions, performed using the same model setup as

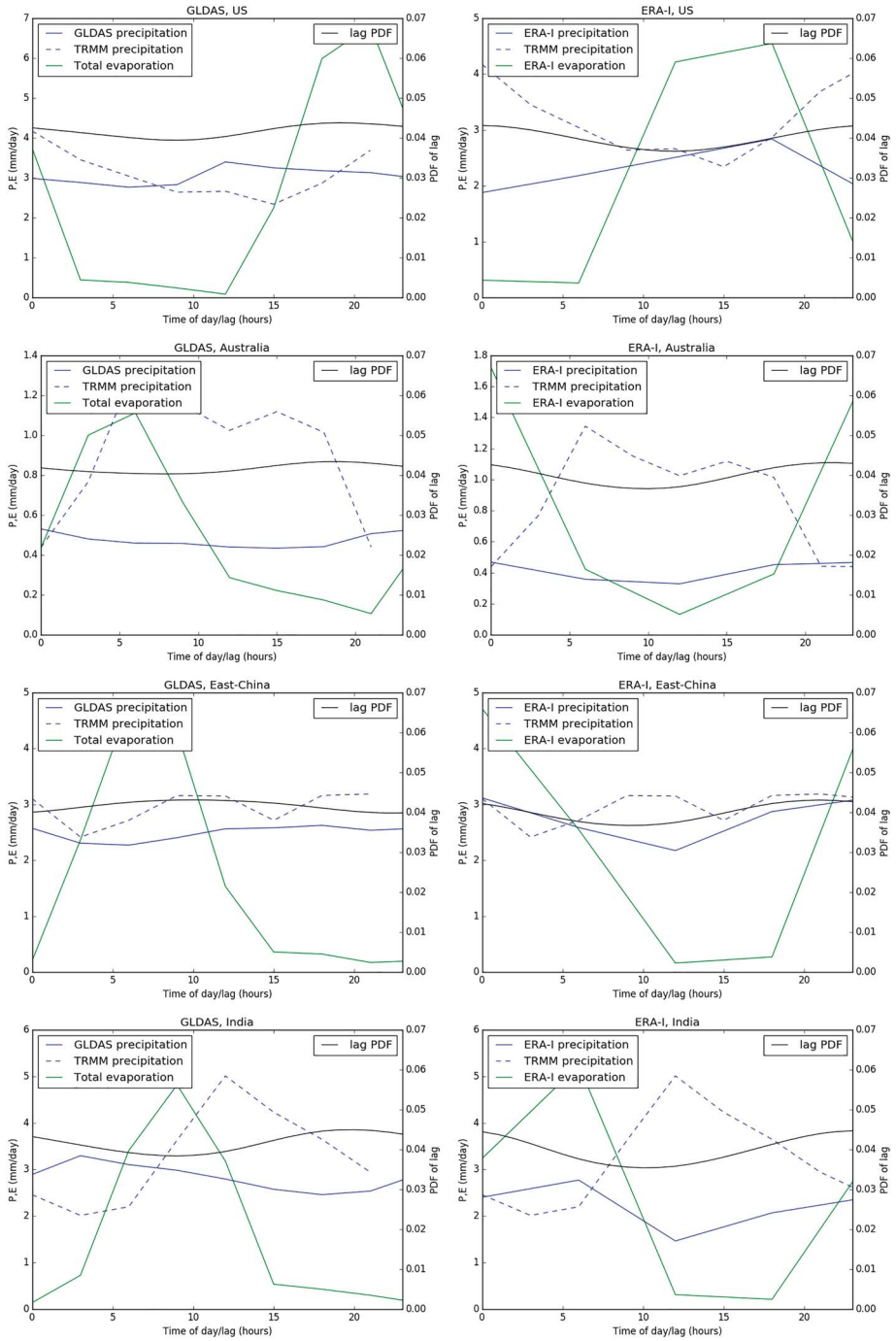

Figure A2. Precipitation (blue lines) and evaporation (green lines) products for the GLDAS (left column) and ERA-I (right column) regions (see Figure A1 for regions), for four regions. (from top to bottom) United States, Australia, East China, and India. Based on precipitation and evaporation, a PDF of the lag between evaporation and precipitation is plotted in black (and on the right axes). ERA-I = ERA-Interim; PDF = probability density function.

in the current study (Staal et al., 2018, and its supplement). For South America, those tests showed a strong influence of convective movement on the moisture recycling ratio during some days, as previously found (Freitas et al., 2000), but quite a small influence on the long-term mean. Given that we are interested in these longer-term means in the current study, we assume that not including this vertical redistribution of moisture does not impact our conclusions.

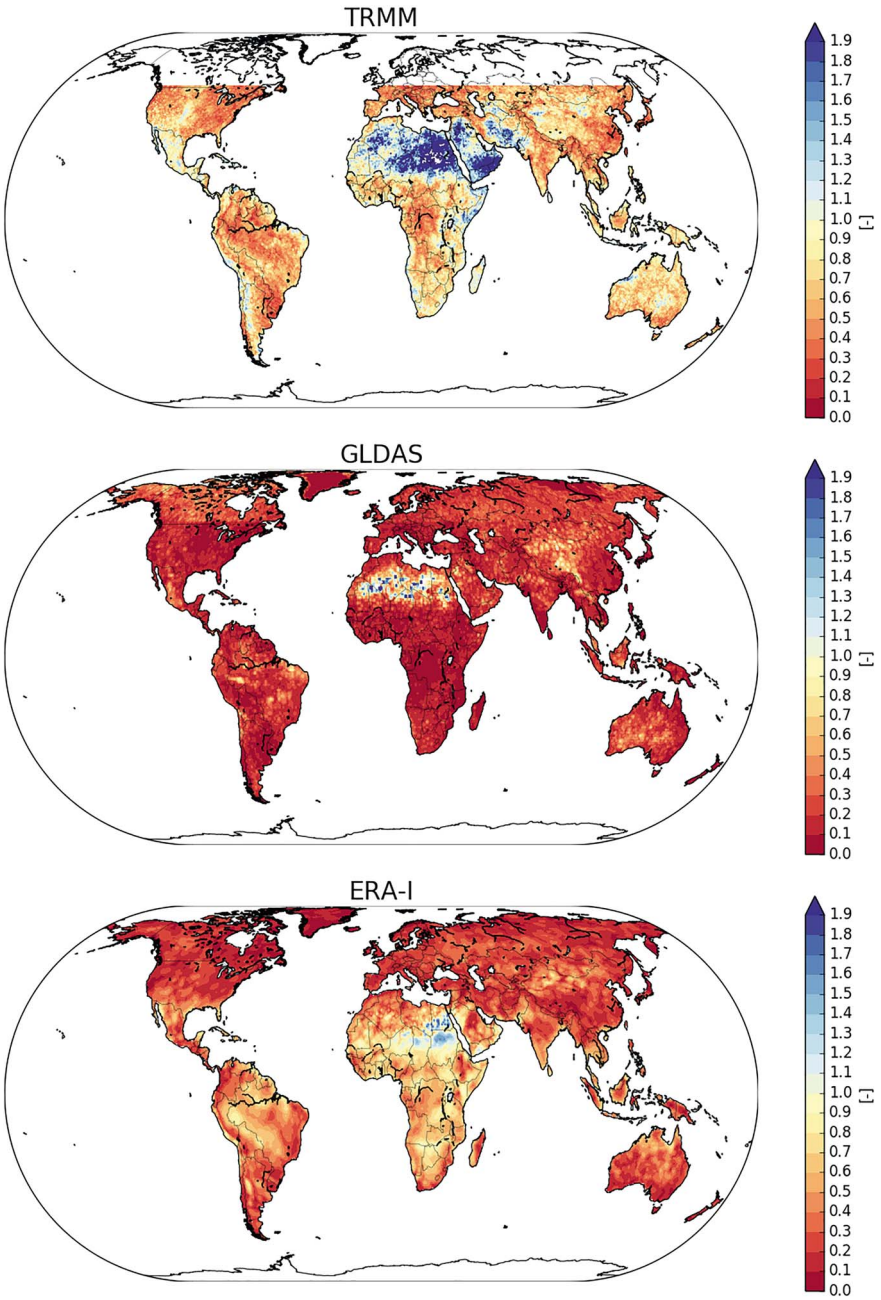

Figure A3. Coefficient of variation of daily cycles of precipitation for TRMM (top panel), GLDAS (middle panel), and ERA-I (bottom panel). ERA-I = ERA-Interim.

5. Conclusion

Based on a previous study of the PDF of atmospheric residence time of evaporation (Van der Ent & Tuinenburg, 2017), we observed that in ERA-I, there appears to be a strong daily cycle in the atmospheric residence time of land evaporation and that there is a difference in general shape of the atmospheric residence time PDFs of oceanic and land evaporation. The current paper tries to infer the processes that cause these phenomena by forcing a Lagrangian three-dimensional moisture tracking scheme with (I) GLDAS and (II) MERRA2 surface fluxes.

We found a much weaker daily cycle in the atmospheric residence time PDF when the moisture tracking model was forced with GLDAS and MERRA2 surface fluxes than when it was forced with the ERA-I surface fluxes. Especially in the tropics, the diurnal cycles of evaporation and precipitation differ between GLDAS

and ERA-I. For regions in the Congo and Amazon basin, evaporation and precipitation peak at noon for ERA-I, while GLDAS has a more distributed diurnal cycle of precipitation and an evaporation peak later during the afternoon. These coinciding diurnal cycles of evaporation and precipitation cause the strong daily cycle in atmospheric residence time PDF in ERA-I, as this daily cycle is a lot weaker based on the GLDAS results, that have a different diurnal cycle of evaporation and precipitation. Moreover, the daily cycle in the MERRA2 data is not present when aggregated globally. Therefore, we conclude that the strong daily cycle found by Van der Ent and Tuinenburg (2017) is probably an artifact of the ERA-I surface flux forcing.

We analyzed the shape of the atmospheric residence time PDF using fits to a gamma function. The previous study found this PDF to be almost strictly decreasing with time for oceanic evaporation, with shape component $\alpha = 1.04$ and increasing during the first few days before decreasing for land evaporation, corresponding to shape components $\alpha = 1.15$. Based on the GLDAS-forced moisture tracking, we found similar gamma distribution shape factors for atmospheric residence time PDFs as for the ERA-I-forced moisture tracking, while the MERRA2 shape factors are different in some areas. Furthermore, we found the transpiration component to be most responsible for this typical shape factors over land, which is confirmed by the MERRA2 simulations, despite different shape factors in some locations. Although we found this high values of the shape factor α globally, it is especially high during the summer season. The cause of these differently shaped PDFs is that the chance of precipitation in the 2 days after an evaporation event is lower if that evaporation is transpiration than when it is canopy evaporation or bare soil evaporation. Therefore, we conclude that the transpiration processes are creating the differences between oceanic and land evaporation atmospheric residence time PDFs.

Appendix A: Diurnal Cycle of Land Surface Fluxes in ERA-Interim and GLDAS: Additional Regions

In addition to the two regions (Congo and Amazon) for which the land surface fluxes daily cycles showed different amplitudes, we repeat this analysis for four regions for which the atmospheric residence time PDF have similar daily cycles. The outline of regions (in parts of the United States, Australia, East China, and India) are plotted in Figure A1. Figure A2 shows the precipitation and evaporation daily cycles for these four regions. The lag PDF is calculated similar to Figure 5.

The overestimation of the amplitude of the daily cycle of precipitation for ERA-I compared to TRMM is not present in any of these four regions, although the timing of the peak is often different. For GLDAS, the daily cycle of precipitation is slightly smaller than that of ERA-I and TRMM.

To test how this daily cycle of precipitation is represented globally, Figure A3 shows the coefficient of variation of the daily cycle of precipitation (standard deviation divided by the mean for the precipitation curves in Figure A2) for TRMM, ERA-I, and GLDAS. Despite the mismatch in size of the precipitation daily cycle between ERA-I and TRMM for the Congo and Amazon cases, the coefficient of variation of the daily cycle in the tropics is quite similar for ERA-I and TRMM. Outside the tropics, but up to the TRMM limits of 50° S–50° N, the daily cycle in ERA-I is smaller than that of TRMM. The daily cycle of precipitation in GLDAS is smaller than in the other data sets. As in the examples in this study, GLDAS precipitation is distributed throughout the day for large parts of the world.

Acknowledgments
This study used ERA-Interim (available at https://www.ecmwf.int/en/forecasts/datasets/archive-datasets/reanalysis-datasets/era-interim), GLDAS (available at https://mirador.gsfc.nasa.gov/cgi-bin/mirador/collectionlist.pl?keyword=GLDAS), TRMM (available at https://mirador.gsfc.nasa.gov/cgi-bin/mirador/collectionlist.pl?keyword=TRMM_3B42), and MERRA (available at https://mirador.gsfc.nasa.gov/cgi-bin/mirador/collectionlist.pl?keyword=MERRA) datasets. We thank their providers. This work is part of the research program Innovational Research Incentives Scheme with project numbers 016.veni.171.019 and 016.veni.181.015, which is financed by the Netherlands Organisation for Scientific Research (NWO).

References

Benettin, P., Soulsby, C., Birkel, C., Tetzlaff, D., Botter, G., & Rinaldo, A. (2017). Using SAS functions and high-resolution isotope data to unravel travel time distributions in headwater catchments. *Water Resources Research*, *53*, 1864–1878. https://doi.org/10.1002/2016WR020117

Berghuijs, W. R., & Kirchner, J. W. (2017). The relationship between contrasting ages of groundwater and streamflow. *Geophysical Research Letters*, *44*, 8925–8935. https://doi.org/10.1002/2017GL074962

Betts, A. K., & Jakob, C. (2002). Evaluation of the diurnal cycle of precipitation, surface thermodynamics, and surface fluxes in the ECMWF model using LBA data. *Journal of Geophysical Research*, *107*(D20), 8045.

Blyth, E., Gash, J., Lloyd, A., Pryor, M., Weedon, G. P., & Shuttleworth, J. (2010). Evaluating the JULES land surface model energy fluxes using FLUXNET data. *Journal of Hydrometeorology*, *11*(2), 509–519.

Bodnar, R. J., Azbej, T., Becker, S. P., Cannatelli, C., Fall, A., & Severs, M. J. (2013). Whole Earth geohydrologic cycle, from the clouds to the core: The distribution of water in the dynamic Earth system. In M. E. Bickford (Ed.), *The web of geological sciences: Advances, impacts, and interactions* (pp. 431–461). Boulder, CO: The Geological Society of America.

Bony, S., Stevens, B., Frierson, D. M., Jakob, C., Kageyama, M., Pincus, R., et al. (2015). Clouds, circulation and climate sensitivity. *Nature Geoscience*, *8*(4), 261.

Bosilovich, M. G., & Schubert, S. D. (2002). Water vapor tracers as diagnostics of the regional hydrologic cycle. *Journal of Hydrometeorology*, *3*(2), 149–165.
Chow, V. T., Maidment, D. R., & Mays, L. W. (1988). *Applied hydrology*. Singapore: McGraw-Hill. 572.
Coenders-Gerrits, A. M. J., Van der Ent, R. J., Bogaard, T. A., Wang-Erlandsson, L., Hrachowitz, M., & Savenije, H. H. G. (2014). Uncertainties in transpiration estimates. *Nature*, *506*(7487), E1—E2.
Dai, A., Giorgi, F., & Trenberth, K. E. (1999). Observed and model-simulated diurnal cycles of precipitation over the contiguous United States. *Journal of Geophysical Research*, *104*(D6), 6377–6402.
Dee, D. P., Uppala, S. M., Simmons, A. J., Berrisford, P., Poli, P., Kobayashi, S., et al. (2011). The ERA-Interim reanalysis: Configuration and performance of the data assimilation system. *Quarterly Journal of the Royal Meteorological Society*, *137*(656), 553–597.
Dirmeyer, P. A., & Brubaker, K. L. (2007). Characterization of the global hydrologic cycle from a back-trajectory analysis of atmospheric water vapor. *Journal of Hydrometeorology*, *8*(1), 20–37.
Dirmeyer, P. A., Cash, B. A., Kinter, J. L., Jung, T., Marx, L., Satoh, M., et al. (2012). Simulating the diurnal cycle of rainfall in global climate models: Resolution versus parameterization. *Climate Dynamics*, *39*(1–2), 399–418.
Dirmeyer, P. A., Gao, X., Zhao, M., Guo, Z., Oki, T., & Hanasaki, N. (2006). GSWP-2: Multimodel analysis and implications for our perception of the land surface. *Bulletin of the American Meteorological Society*, *87*(10), 1381–1397.
Eyring, V., Bony, S., Meehl, G. A., Senior, C. A., Stevens, B., Stouffer, R. J., & Taylor, K. E. (2016). Overview of the Coupled Model Intercomparison Project Phase 6 (cmip6) experimental design and organization. *Geoscientific Model Development*, *9*(5), 1937–1958.
Fisher, J. B., Melton, F., Middleton, E., Hain, C., Anderson, M., Allen, R., et al. (2017). The future of evapotranspiration: Global requirements for ecosystem functioning, carbon and climate feedbacks, agricultural management, and water resources. *Water Resources Research*, *53*, 2618–2626. https://doi.org/10.1002/2016WR020175
Freitas, S., Dias, M. S., Dias, P. S., Longo, K., Artaxo, P., Andreae, M., & Fischer, H. (2000). A convective kinematic trajectory technique for low-resolution atmospheric models. *Journal of Geophysical Research*, *105*(D19), 24,375–24,386.
Gelaro, R., McCarty, W., Suárez, M. J., Todling, R., Molod, A., Takacs, L., et al. (2017). The Modern-Era Retrospective Analysis for Research and Applications, version 2 (MERRA-2). *Journal of Climate*, *30*(14), 5419–5454.
Hrachowitz, M., Soulsby, C., Tetzlaff, D., Malcolm, I., & Schoups, G. (2010). Gamma distribution models for transit time estimation in catchments: Physical interpretation of parameters and implications for time-variant transit time assessment. *Water Resources Research*, *46*, W10536. https://doi.org/10.1029/2010WR009148
Huffman, G. J., Bolvin, D. T., Nelkin, E. J., Wolff, D. B., Adler, R. F., Gu, G., et al. (2007). The TRMM Multisatellite Precipitation Analysis (TMPA): Quasi-global, multiyear, combined-sensor precipitation estimates at fine scales. *Journal of Hydrometeorology*, *8*(1), 38–55.
Jones, J. A. A. (1997). *Global hydrology: Processes, resources and environmental management* (399 pp.). Harlow: Longman.
Keys, P. W., Barnes, E. A., van der Ent, R. J., & Gordon, L. J. (2014). Variability of moisture recycling using a precipitationshed framework. *Hydrology and Earth System Sciences*, *18*(10), 3937.
Läderach, A., & Sodemann, H. (2016). A revised picture of the atmospheric moisture residence time. *Geophysical Research Letters*, *43*, 924–933. https://doi.org/10.1002/2015GL067449
McGuire, K. J., & McDonnell, J. J. (2006). A review and evaluation of catchment transit time modeling. *Journal of Hydrology*, *330*(3–4), 543–563.
Rienecker, M. M., Suarez, M. J., Gelaro, R., Todling, R., Bacmeister, J., Liu, E., et al. (2011). MERRA: NASA's Modern-Era Retrospective Analysis for Research and Applications. *Journal of climate*, *24*(14), 3624–3648.
Rodell, M., Houser, P. R., Jambor, U. E. A., Gottschalck, J., Mitchell, K., Meng, C. J., et al. (2004). The global land data assimilation system. *Bulletin of the American Meteorological Society*, *85*(3), 381–394.
Schlesinger, W. H., & Jasechko, S. (2014). Transpiration in the global water cycle. *Agricultural and Forest Meteorology*, *189*, 115–117.
Shaw, T., Baldwin, M., Barnes, E., Caballero, R., Garfinkel, C., Hwang, Y.-T., et al. (2016). Storm track processes and the opposing influences of climate change. *Nature Geoscience*, *9*(9), 656.
Staal, A., Tuinenburg, O. A., Bosmans, J. H., Holmgren, M., van Nes, E. H., Scheffer, M., et al. (2018). Forest-rainfall cascades buffer against drought across the Amazon. *Nature Climate Change*, *8*, 539–543.
Sutanto, S. J., Van den Hurk, B., Dirmeyer, P. A., Seneviratne, S. I., Röckmann, T., Trenberth, K. E., et al. (2014). Hess opinions "a perspective on isotope versus non-isotope approaches to determine the contribution of transpiration to total evaporation". *Hydrology and Earth System Sciences*, *18*(8), 2815.
Trenberth, K. E. (1998). Atmospheric moisture residence times and cycling: Implications for rainfall rates and climate change. *Climate Change*, *39*(4), 667–694.
Trenberth, K. E., Dai, A., Rasmussen, R. M., & Parsons, D. B. (2003). The changing character of precipitation. *Bulletin of the American Meteorological Society*, *84*(9), 1205–1217.
Tuinenburg, O. A., Hutjes, R. W. A., & Kabat, P. (2012). The fate of evaporated water from the Ganges basin. *Journal of Geophysical Research*, *117*, D01107. https://doi.org/10.1029/2011JD016221
Van der Ent, R. J., & Savenije, H. H. G. (2011). Length and time scales of atmospheric moisture recycling. *Atmospheric Chemistry and Physics*, *11*(5), 1853–1863.
Van der Ent, R. J., & Savenije, H. H. (2013). Oceanic sources of continental precipitation and the correlation with sea surface temperature. *Water Resources Research*, *49*, 3993–4004. https://doi.org/10.1002/wrcr.20296
Van der Ent, R. J., & Tuinenburg, O. A. (2017). The residence time of water in the atmosphere revisited. *Hydrology and Earth System Sciences*, *21*, 779–790.
Van der Ent, R., Tuinenburg, O., Knoche, H.-R., Kunstmann, H., & Savenije, H. (2013). Should we use a simple or complex model for moisture recycling and atmospheric moisture tracking? *Hydrology and Earth System Sciences*, *17*(12), 4869–4884.
Van der Ent, R. J., Wang-Erlandsson, L., Keys, P. W., & Savenije, H. H. G. (2014). Contrasting roles of interception and transpiration in the hydrological cycle—Part 2: Moisture recycling. *Earth System Dynamics*, *5*(2), 471–489.
Wang-Erlandsson, L., Bastiaanssen, W. G. M., Gao, H., Senay, G. B., van Dijk, A. I. J. M., Guerschman, J. P., et al. (2016). Global root zone storage capacity from satellite-based evaporation. *Hydrology and Earth System Sciences*, *2016*(1), 1–1.
Ward, R. C., & Robinson, M. (2000). *Principles of hydrology* (450 pp.). Berkshire: McGraw-Hill.
Wei, J., Knoche, H. R., & Kunstmann, H. (2016). Atmospheric residence times from transpiration and evaporation to precipitation: An age-weighted regional evaporation tagging approach. *Journal of Geophysical Research: Atmospheres*, *121*, 6841–6862. https://doi.org/10.1002/2015JDO24650
Yoshimura, K., Oki, T., & Ichiyanagi, K. (2004). Evaluation of two-dimensional atmospheric water circulation fields in reanalyses by using precipitation isotopes databases. *Journal of Geophysical Research*, *109*, D20109. https://doi.org/10.1029/2004JD004764